

Temperature-pressure phase diagram of the ferromagnetic Kondo lattice compound CePtAl₄Si₂

Honghong Wang,^{1,*} Tae Beom Park,^{1,2,*} Soohyeon Shin^{①,1,3}, Jihyun Kim,^{1,2} Hanoh Lee,¹ and Tuson Park^{1,†}

¹*Center for Quantum Materials and Superconductivity (CQMS) and Department of Physics, Sungkyunkwan University, Suwon 16419, South Korea*

²*Institute of Basic Science, Sungkyunkwan University, Suwon 16419, South Korea*

³*Laboratory for Multiscale Materials Experiments, Paul Scherrer Institut, CH-5232 Villigen PSI, Switzerland*



(Received 14 March 2023; revised 25 May 2023; accepted 10 July 2023; published 21 July 2023)

Ferromagnetic (FM) systems have attracted interest because a variety of novel phases can arise near a quantum critical point (QCP) where the FM order is suppressed to zero temperature. The Kondo lattice compound CePtAl₄Si₂ is a candidate FM quantum critical material that becomes the FM state below $T_c = 3.7$ K, but the possibility of the quantum criticality has yet to be studied. Here, we report a comprehensive temperature-pressure phase diagram of CePtAl₄Si₂ using a systematic transport investigation. The FM compound CePtAl₄Si₂ goes through three distinct ground states under pressure. In the low-pressure FM state, T_c is gradually suppressed by pressure and a smooth extrapolation of $T_c(P)$ reaches zero temperature at a critical pressure of 7.0 GPa. However, the suppression of T_c is interrupted by the appearance of another crossover temperature T^* in the intermediate pressure range of 5.4–11.7 GPa, which shows a nonmonotonic pressure dependence. A fully coherent Kondo screened state is observed in the high-pressure regime. These results suggest that a FM QCP is avoided under pressure in the disordered Kondo system CePtAl₄Si₂.

DOI: [10.1103/PhysRevMaterials.7.075003](https://doi.org/10.1103/PhysRevMaterials.7.075003)

I. INTRODUCTION

The quantum critical point (QCP) emerges when a second-order magnetic phase transition is continuously suppressed to zero temperature by a nonthermal tuning parameter. It has been extensively explored in several classes of materials owing to the appearance of fascinating phenomena in the proximity of the quantum critical regime, such as unconventional superconductivity and non-Fermi-liquid behavior [1–3]. In many antiferromagnetic (AFM) systems, the continuous suppression of AFM order terminates at a QCP [4–6]. However, a variety of phase diagrams have been revealed in the ferromagnetic (FM) systems [7]. For example, the FM QCP is avoided in most of the clean FM systems as the systems approach the critical point. The nature of the FM transition may change from second to first order at a tricritical point where tricritical wings emerge upon the application of a magnetic field that terminate at quantum critical end points in the temperature-pressure-magnetic field phase diagram [8–11]. The FM transition can also be replaced by the appearance of a modulated magnetic phase [12–17]. Another interesting scenario is the coexistence of tricritical wings and modulated magnetic phases [18]. If the tricritical point is suppressed by increasing disorder, the tricritical point could merge with the quantum critical end points and a FM QCP may appear at zero magnetic field [19,20]. Indeed, such a continuous FM transition to zero temperature, corresponding to a FM QCP, has been found in the disordered systems tuned by substitution [21–25]. Recently, a pressure-induced FM QCP has been

reported even in the pure FM Kondo lattice CeRh₆Ge₄ with a quasi-one-dimensional crystal structure [26], indicating that it remains a challenging issue to understand the complex phase diagrams in FM systems.

CePtAl₄Si₂ belongs to the family of CeT_nAl_{2n+2}Si₂ ($T = \text{Rh, Ir, Pt}$) systems with $n = 1$, which crystallizes in the tetragonal KCu₄S₃-type structure with the space group $P4/mmm$ and consists of sequential stacking of Ce-containing BaAl₄-type layers separated by TAl₂-type slabs along the c axis [27]. In contrast to the AFM ground state in CeRhAl₄Si₂ and CeIrAl₄Si₂, the anomalies in the transport, specific heat, and susceptibility measurements indicate that CePtAl₄Si₂ becomes the FM state below $T_c = 3.7$ K with the moments aligned in the basal plane at ambient pressure [27]. Herein, we report the comprehensive temperature-pressure (T - P) phase diagram of CePtAl₄Si₂ using transport measurements under high pressure. By applying pressure, the signature of T_c in the resistivity, namely, a peak behavior, is gradually suppressed and disappears at around 4.1 GPa. Above this pressure, a kink anomaly emerges at T^* and the resistivity shows a negative temperature dependence over the entire temperature range, which persists up to 11.7 GPa. As the pressure is further increased, a fully coherent Kondo state, which is absent at ambient pressure, begins to develop above 14.0 GPa.

II. EXPERIMENT METHODS

Single crystals of CePtAl₄Si₂ were synthesized using the Al/Si eutectic flux method as described elsewhere [27,28]. Most of the excess Al/Si eutectic flux was removed using a centrifuge at 700 °C before cooling down to room temperature during the syntheses. A slight trace of the flux stuck to the

*These authors contributed equally to this work.

†Corresponding author: tp8701@skku.edu

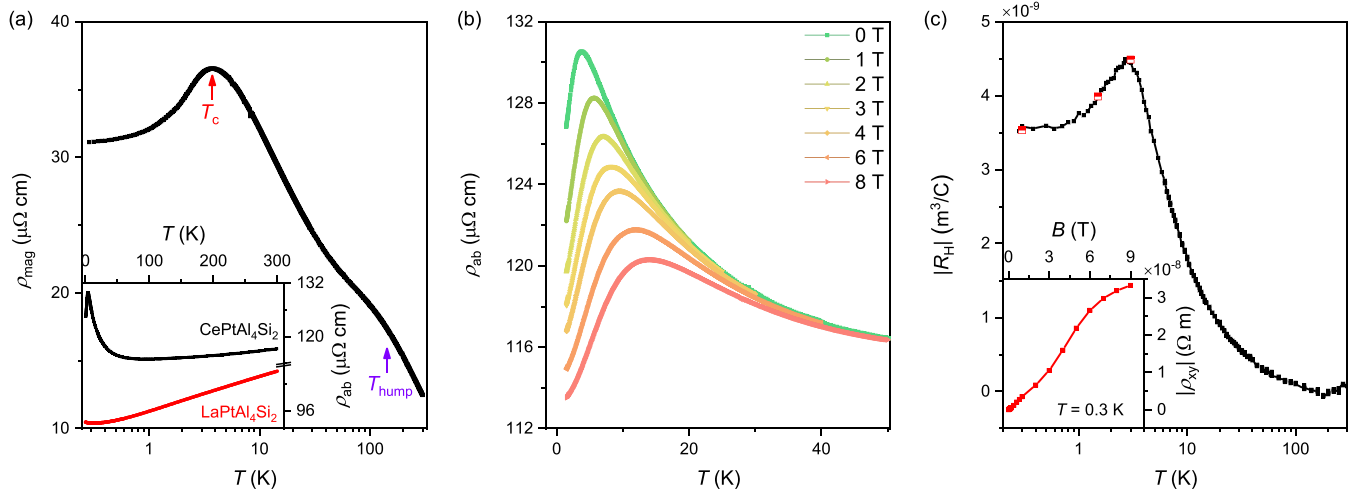


FIG. 1. (a) Temperature dependence of the magnetic resistivity $\rho_{\text{mag}}(T)$ for $\text{CePtAl}_4\text{Si}_2$ at ambient pressure. The violet and red arrows mark the resistivity hump temperature T_{hump} and the onset temperature of FM order T_c , respectively. The inset shows the electrical resistivity $\rho_{\text{ab}}(T)$ for $\text{CePtAl}_4\text{Si}_2$ (black symbols) and its nonmagnetic analog $\text{LaPtAl}_4\text{Si}_2$ (red symbols). (b) Temperature dependence of the in-plane resistivity $\rho_{\text{ab}}(T)$ for $\text{CePtAl}_4\text{Si}_2$ measured at various fields applied along the in-plane direction. (c) Temperature dependence of the Hall coefficient $R_{\text{H}}(T)$ for $\text{CePtAl}_4\text{Si}_2$ measured at a field of 1 T applied along the c axis. The red symbols represent the Hall coefficient R_{H} obtained from the initial slope of the isothermal field-dependent Hall resistivity $\rho_{\text{xy}}(B)$, as shown in the inset.

crystal surface was further removed by polishing the sample surface with sandpaper before the transport measurements. A representative powder x-ray diffraction pattern of $\text{CePtAl}_4\text{Si}_2$ is shown in the Supplemental Material, Fig. S1 [29], along with the Rietveld refinement, confirming the tetragonal crystal structure with the space group $P4/mmm$. Resistivity and Hall measurements at ambient pressure were performed using the standard six-probe method on a rectangular platelet with spot-welded contacts. Pressure work was conducted in a diamond-anvil cell made of Be-Cu alloy with NaCl powder as the pressure-transmitting medium to obtain a quasi-hydrostatic pressure environment. The van der Pauw method was used for the high-pressure transport measurements [30]. The pressure in the diamond-anvil cell was determined using the ruby fluorescence method [31]. Field inversion was used to eliminate the longitudinal magnetoresistance contribution owing to misalignment during the isothermal field and the temperature dependence of the Hall resistivity measurements. All measurements were performed with a low-frequency resistance bridge in a ^4He cryostat from 300 to 1.5 K and a HelioxVL system from 10 to 0.3 K.

III. RESULTS AND DISCUSSION

Figure 1(a) displays the temperature dependence of the in-plane magnetic resistivity $\rho_{\text{mag}}(T)$ for $\text{CePtAl}_4\text{Si}_2$ at ambient pressure, which was obtained by subtracting the phonon-scattering contribution estimated by the resistivity $\rho_{\text{ab}}(T)$ of the nonmagnetic analog $\text{LaPtAl}_4\text{Si}_2$ [see inset of Fig. 1(a)]. $\rho_{\text{mag}}(T)$ exhibits two anomalies at $T_{\text{hump}} \approx 150$ K and $T_c = 3.7$ K. Above the two characteristic temperatures, $\rho_{\text{mag}}(T)$ follows a logarithmic T dependence owing to incoherent Kondo scattering [32,33]. However, the rapid drop of $\rho_{\text{mag}}(T)$ below T_c is not associated with the formation of coherent Kondo scattering shown in typical metallic heavy fermion compounds [32,33] but arises from the reduction of spin scattering in-

duced by the formation of FM order [27]. The maximum temperature T_c moves to higher temperatures when subjected to a magnetic field applied along the in-plane direction, as shown in Fig. 1(b), which further supports that the peak at T_c is of magnetic origin. The absolute value of the Hall coefficient $|R_{\text{H}}|$, which was obtained under a field of 1 T applied along the c axis, is plotted as a function of temperature in Fig. 1(c). At temperatures below 150 K, $|R_{\text{H}}|$ shows a rapid increase with decreasing temperature and reaches a local maximum at 3.0 K, below which it begins to decrease with further decreasing temperature. Meanwhile, the field dependence of the Hall resistivity $\rho_{\text{xy}}(B)$ was measured at several temperatures [inset of Fig. 1(c)]. Despite the nonlinear field dependence of $\rho_{\text{xy}}(B)$, the R_{H} values derived from the initial slope of $\rho_{\text{xy}}(B)$, denoted by the red symbols in Fig. 1(c), are consistent with the R_{H} determined at 1 T.

Figure 2 shows the temperature dependence of the in-plane resistivity $\rho_{\text{ab}}(T)$ for $\text{CePtAl}_4\text{Si}_2$ at various pressures up to 26.5 GPa. The onset of magnetic order, signified by the local maximum of $\rho_{\text{ab}}(T)$, is observed at pressures below 4.1 GPa, as shown in Fig. 2(a). Along with the suppression of T_c , the peak related to T_c is weakened with increasing pressure and disappears at 5.4 GPa where a kink appears at T^* and is identified by the intercrossing of two violet dashed lines in the inset of Fig. 2(a). As the temperature decreases further below T^* , $\rho_{\text{ab}}(T)$ increases, but with a smaller slope. Figure 2(b) shows $\rho_{\text{ab}}(T)$ for selective pressures of 8.4, 10.7, and 11.7 GPa, where the resistivity increases with decreasing temperature in the entire temperature range. As pressure increases to 14.5 GPa, as shown in Figs. 2(c) and 2(d), $\rho_{\text{ab}}(T)$ decreases with temperature below T_{coh} and exhibits a temperature-squared dependence as $\rho_{\text{ab}}(T) = \rho_0 + AT^2$, suggesting that the system enters the Fermi-liquid ground state. At higher pressures, T_{coh} increases with increasing pressure. Observations of the peak temperature T_{coh} in $\rho_{\text{ab}}(T)$ and the low-temperature Fermi-liquid behavior suggest that T_{coh} is

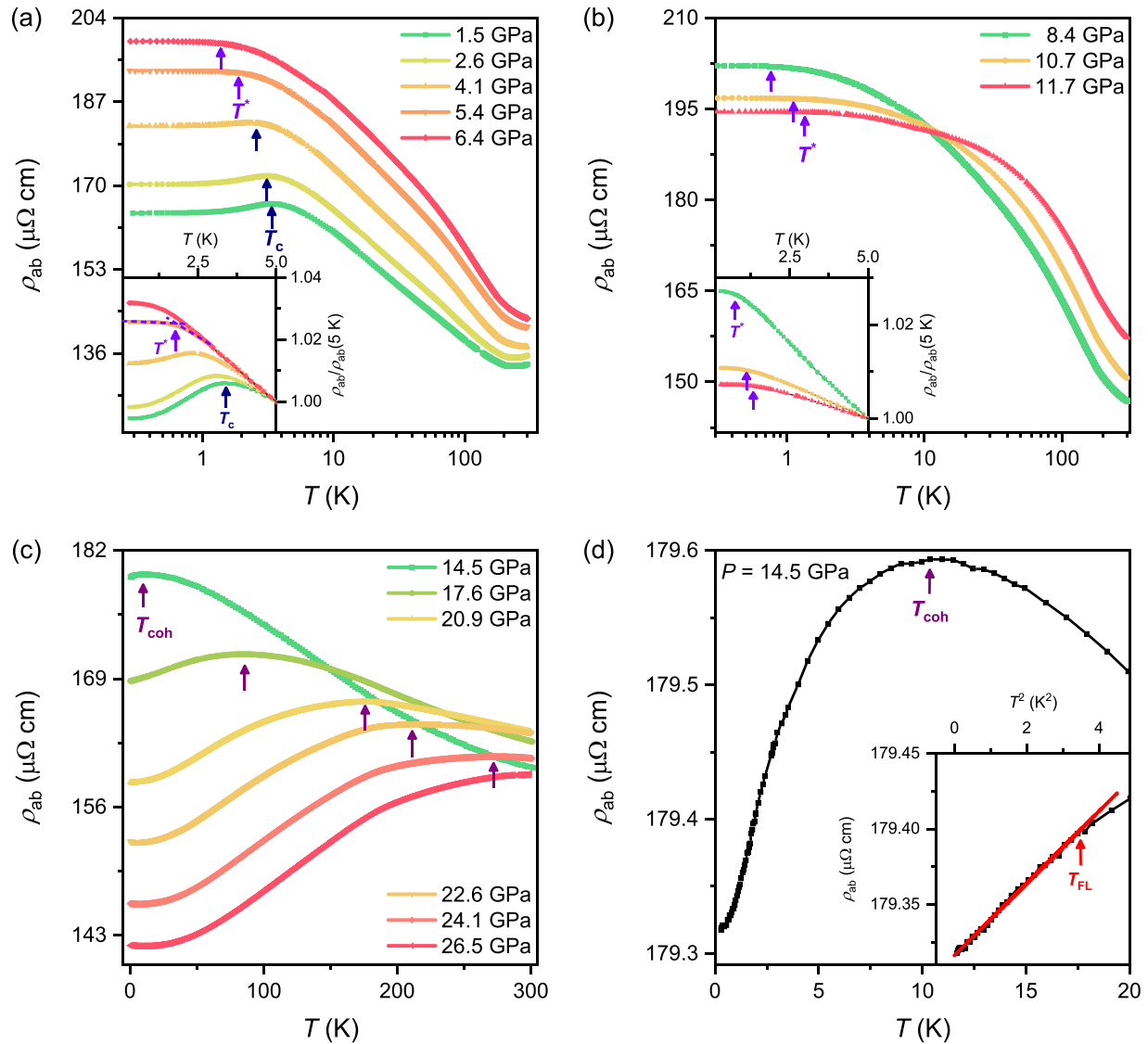


FIG. 2. (a)–(c) Temperature dependence of the in-plane resistivity $\rho_{ab}(T)$ for $\text{CePtAl}_4\text{Si}_2$ at various pressures. The insets of (a), (b) show enlarged views of the normalized resistivity $\rho_{ab}/\rho_{ab}(5\text{ K})$ in the low-temperature range. The dashed violet lines in the inset of (a) are visual guides. The navy and violet arrows in (a), (b) indicate the onset temperature of FM order T_c and kink temperature T^* , respectively. The purple arrows in (c) represent the coherent temperature T_{coh} . (d) The enlarged views of the low-temperature resistivity $\rho_{ab}(T)$ at 14.5 GPa. The inset of (d) shows the least-squares fit to the low-temperature data of the form $\rho_{ab}(T) = \rho_0 + AT^2$. The red and purple arrows in (d) denote the onset temperature of Fermi-liquid behavior T_{FL} and T_{coh} , respectively.

associated with the onset of Kondo coherence in metallic Kondo lattice systems [32,33]. We note that a low-temperature upturn in resistivity appears above 20 GPa (see Fig. S2 in the Supplemental Material [29] for more details). The positive magnetoresistance rules out the conventional explanation of weak localization for the increase in resistivity (see Fig. S3 in the Supplemental Material [29] for the magnetoresistance results under pressure).

Figure 3 shows the low-temperature Hall coefficient $|R_H|$ of $\text{CePtAl}_4\text{Si}_2$ at 1 T, where the characteristic features revealed in $\rho_{ab}(T)$ are reflected in $R_H(T)$. In the low-pressure regime below 4.1 GPa, $|R_H|$ reaches a maximum near T_c and the maximum temperature decreases with increasing pressure. This behavior is in accordance with the suppression of T_c observed in $\rho_{ab}(T)$ under pressure. In the intermediate

pressure range of 5.4–11.7 GPa, a kink appears in $R_H(T)$ and $|R_H|$ monotonically increases with decreasing temperature as shown in $\rho_{ab}(T)$. In the high-pressure regime above 11.7 GPa, $R_H(T)$ gradually flattens as the pressure increases. The Hall resistivity measured as a function of the field $\rho_{xy}(B)$ at $T = 0.3\text{ K}$, as shown in Fig. 4, remains nonlinear in the field up to 11.7 GPa and exhibits a linear field dependence above it. The linear field-dependent $\rho_{xy}(B)$ is consistent with the low-temperature Fermi-liquid behavior in $\rho_{ab}(T)$ [34,35].

The comprehensive T - P phase diagram from the resistivity measurements for $\text{CePtAl}_4\text{Si}_2$ is summarized in Fig. 5(a). Three main regions are identified, which correspond to the ferromagnetic (FM), intermediate (IM), and coherent (CH) states. In the low-pressure FM phase, as a function of the pressure, T_c is gradually suppressed from 3.7 K at $P = 0\text{ GPa}$

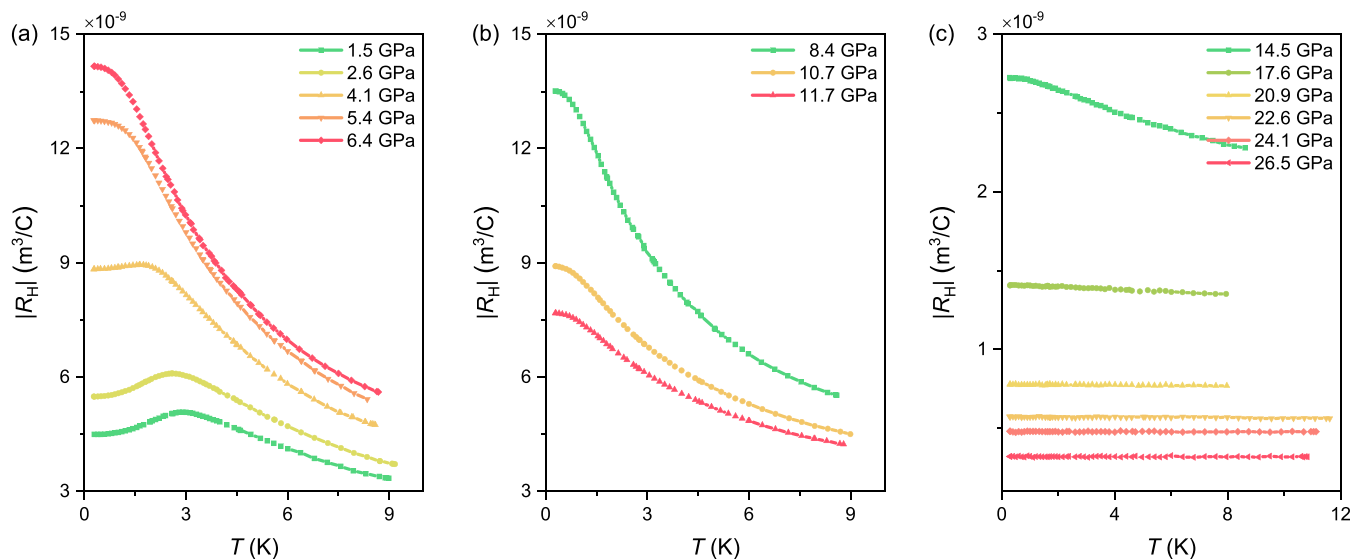


FIG. 3. (a)–(c) Temperature dependence of the Hall coefficient $R_H(T)$ for $\text{CePtAl}_4\text{Si}_2$ at various pressures measured under a magnetic field of 1.0 T along the c axis.

to 2.4 K at $P = 4.1$ GPa. A smooth extrapolation of $T_c(P)$ to $T = 0$ K suggests that the FM transition is suppressed at the critical pressure point P_{c1} near 7.0 GPa. Additional evidence for the suppression of the FM order near P_{c1} is obtained from the low-temperature properties. Figure 5(b) shows that the residual resistivity ρ_0 , which is estimated by the resistivity at 0.3 K, reaches a maximum near P_{c1} . The enhancement in ρ_0 is often observed in the vicinity of the quantum phase transition and ascribed to the magnetic fluctuations. In accordance with the suppression of the FM order, the magnitude of the magnetoresistance measured at 0.3 K and 8 T reaches a maximum near P_{c1} [36]. However, at pressures above 4.1 GPa, the smooth suppression of T_c is interrupted by the appearance of T^* , which decreases when the pressure is further increased to 6.4 GPa and then increases from 0.76 K at $P = 8.4$ GPa to

1.32 K at $P = 11.7$ GPa. At pressures higher than P_{c2} (approximately 14.0 GPa), the system enters a coherent state, manifested by the appearance of low-temperature Fermi-liquid behavior in Fig. 2(d), linear field-dependent $\rho_{xy}(B)$ in Fig. 4(c), and positive magnetoresistance in Fig. 5(b) and Fig. S3 in the Supplemental Material [29].

The lack of coherent Kondo screening at ambient pressure and the delayed Kondo coherence at higher pressures in $\text{CePtAl}_4\text{Si}_2$ are reminiscent of the low-carrier-density systems [37]. For example, similar negative temperature dependence of resistivity behavior and the comparable Hall values have been observed in other low-carrier-density systems such as $\text{Ce}_3\text{Ir}_4\text{Ge}_{13}$ [38] and $\text{Yb}_3\text{Ir}_4\text{Ge}_{13}$ [39]. However, more comprehensive and quantitative analyses are required to make a conclusive statement that $\text{CePtAl}_4\text{Si}_2$ belongs to the family of

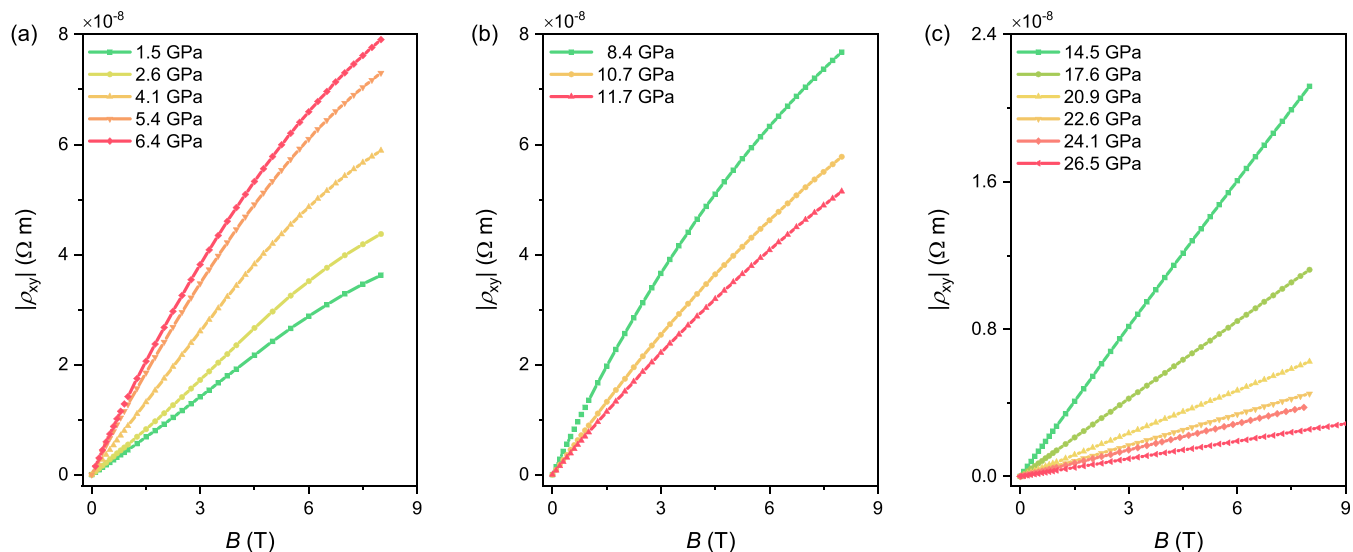


FIG. 4. (a)–(c) Field dependence of the isothermal Hall resistivity $\rho_{xy}(B)$ for $\text{CePtAl}_4\text{Si}_2$ at various pressures measured at 0.3 K and under magnetic field along the c axis.

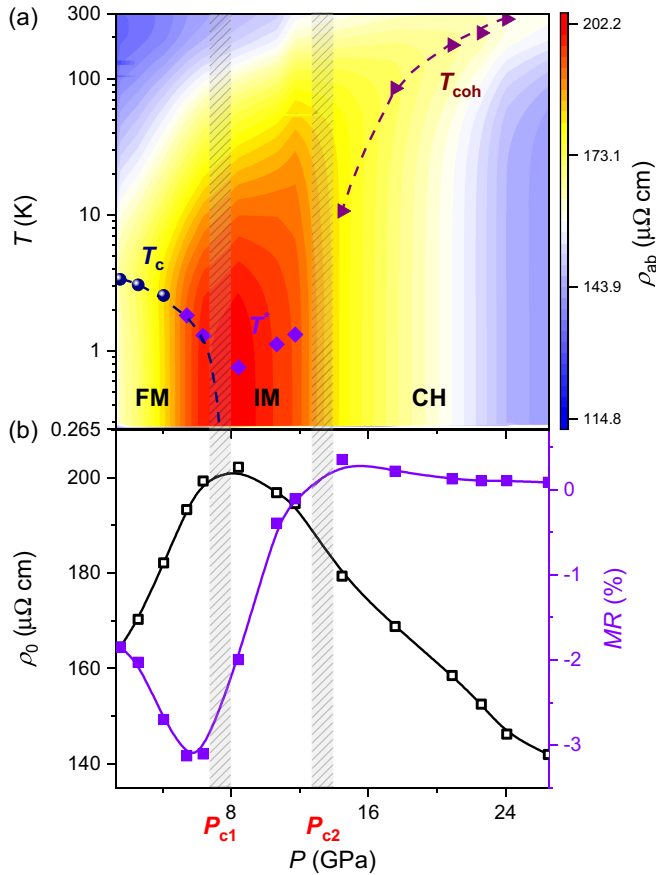


FIG. 5. (a) Temperature-pressure (T - P) phase diagram for $\text{CePtAl}_4\text{Si}_2$. The colors represent the in-plane resistivity $\rho_{ab}(T, P)$. The navy circles, violet diamonds, and purple triangles denote the onset of FM transition T_c , kink temperature T^* , and coherent temperature T_{coh} , respectively. (b) Pressure dependence of the residual resistivity (ρ_0 , black squares) estimated by the resistivity at 0.3 K and the magnetoresistance (MR , violet squares) measured at 0.3 K and 8.0 T, plotted on the left and right ordinates, respectively. The solid and dashed lines are guides to the eyes. FM, IM, and CH denote the ferromagnetic phase, intermediate phase, and coherent state, respectively.

low-carrier-density systems. Another alternative explanation for the lack of Kondo coherence at ambient pressure is the presence of disorder in $\text{CePtAl}_4\text{Si}_2$. As shown in the inset of Fig. 1(a), the resistivity of $\text{LaPtAl}_4\text{Si}_2$ decreases from $104.8 \mu\Omega \text{ cm}$ at room temperature to $93.3 \mu\Omega \text{ cm}$ at 2 K and the residual resistivity ratio (RRR) defined as $\rho_{300\text{K}}/\rho_{2\text{K}}$ is only 1.1, indicating a significant level of disorder in $\text{LaPtAl}_4\text{Si}_2$. Since the disorder in $\text{LaPtAl}_4\text{Si}_2$ is associated with the nonmagnetic elements, e.g., site exchange/nonstoichiometry between Pt and Si positions [27], a similar level of disorder could be expected in the magnetic homologue $\text{CePtAl}_4\text{Si}_2$. The anomaly in the specific heat at the proposed FM transition, which is much broader than those observed for the homologues $\text{CeRhAl}_4\text{Si}_2$ and $\text{CeIrAl}_4\text{Si}_2$, is consistent with the presence of disorder in $\text{CePtAl}_4\text{Si}_2$ [27]. We note that large RRR values of 7.6 and 6.3 for $\text{CeIrAl}_4\text{Si}_2$ and $\text{CeRhAl}_4\text{Si}_2$, respectively, indicate a low level of disorder in the Rh and Ir systems compared to the Pt system [27]. With

the enhancement of the Kondo effect by pressure, the magnetic order is gradually suppressed and the coherent Kondo state develops above P_{c2} . At the highest measured pressure of 26.5 GPa, the coherent Kondo temperature is significantly enhanced. Except for a small increase below 10 K, the resistivity shows a monotonous decrease with decreasing temperature and RRR is approximately 1.1, indicating that the residual resistivity remains large despite a very large onset temperature of Kondo coherence.

The characteristic temperature $T^*(P)$, which appears in the intermediate pressure range of 5.4–11.7 GPa, may correspond to the FM transition below 6.4 GPa, but it may be associated with a modulated magnetic phase, such as a spin-density wave or AFM order, between 8.4 and 11.7 GPa. At pressures below 6.4 GPa, the change in the resistive signature from peak to kink, which corresponds to the evolution from T_c to T^* , appears continuous in Fig. 2(a), implying that T^* is associated with the FM transition. This scenario is corroborated by the observation that $T^*(P)$ is located on the extrapolated line of $T_c(P)$. At pressures above 6.4 GPa, $T^*(P)$ deviates from the extrapolation of $T_c(P)$ and increases with an increase in the pressure. These results suggest that a FM QCP is avoided in $\text{CePtAl}_4\text{Si}_2$ as reported in many FM systems and the deviation of $T^*(P)$ from the extrapolation of $T_c(P)$ may be associated with the appearance of modulated magnetic phases, as observed in CeAgSb_2 [12], CeRuPO [13,14], MnP [15,16], and LaCrGe_3 [17,18]. Further microscopic measurements are necessary to clarify the nature and origin of the temperature scale $T^*(P)$.

IV. CONCLUSION

In summary, a comprehensive T - P phase diagram of the FM Kondo lattice material $\text{CePtAl}_4\text{Si}_2$ has been constructed using transport measurements up to 26.5 GPa. The FM transition is gradually suppressed with the application of pressure, and the vanishing of the FM transition appears to occur near a critical pressure of 7.0 GPa, where the low-temperature resistivity and the magnitude of the magnetoresistance reach a maximum. However, the peak anomaly in the resistivity at the FM transition is replaced by the kink behavior above 4.1 GPa, whose origin requires further investigation. In the high-pressure regime above 14.0 GPa, with the enhancement of the Kondo effect, all the local moments are screened and a coherent Kondo state is formed, leading to a Fermi-liquid behavior. These results demonstrate that a FM QCP is avoided under pressure in the disordered Kondo system $\text{CePtAl}_4\text{Si}_2$, which is different from the disordered systems that display a continuous FM transition tuned by chemical substitution.

ACKNOWLEDGMENTS

This research was supported by Basic Science Research Program through the National Research Foundation of Korea (NRF) funded by the Ministry of Education (Grant No. 2021R1I1A1A01047499) and by the National Research Foundation of Korea (NRF) grant funded by the Korea government (MSIT) (Grants No. 2021R1A2C2010925 and No. 2021R1A2C1014319).

- [1] S. Sachdev, *Quantum Phase Transitions* (Cambridge University Press, Cambridge, 2001).
- [2] G. R. Stewart, Non-Fermi-liquid behavior in d - and f -electron metals, *Rev. Mod. Phys.* **73**, 797 (2001).
- [3] H. v. Löhneysen, A. Rosch, M. Vojta, and P. Wölfle, Fermi-liquid instabilities at magnetic quantum phase transitions, *Rev. Mod. Phys.* **79**, 1015 (2007).
- [4] T. Shibauchi, A. Carrington, and Y. Matsuda, A quantum critical point lying beneath the superconducting dome in iron pnictides, *Annu. Rev. Condens. Matter Phys.* **5**, 113 (2014).
- [5] P. Gegenwart, Q. Si, and F. Steglich, Quantum criticality in heavy-fermion metals, *Nat. Phys.* **4**, 186 (2008).
- [6] Q. Si and F. Steglich, Heavy fermions and quantum phase transitions, *Science* **329**, 1161 (2010).
- [7] M. Brando, D. Belitz, F. M. Grosche, and T. R. Kirkpatrick, Metallic quantum ferromagnets, *Rev. Mod. Phys.* **88**, 025006 (2016).
- [8] C. Pfleiderer, S. R. Julian, and G. G. Lonzarich, Non-Fermi-liquid nature of the normal state of itinerant-electron ferromagnets, *Nature (London)* **414**, 427 (2001).
- [9] M. Uhlarz, C. Pfleiderer, and S. M. Hayden, Quantum Phase Transitions in the Itinerant Ferromagnet $ZrZn_2$, *Phys. Rev. Lett.* **93**, 256404 (2004).
- [10] V. Taufour, D. Aoki, G. Knebel, and J. Flouquet, Tricritical Point and Wing Structure in the Itinerant Ferromagnet UGe_2 , *Phys. Rev. Lett.* **105**, 217201 (2010).
- [11] Y. Shimizu, D. Braithwaite, B. Salce, T. Combier, D. Aoki, E. N. Hering, S. M. Ramos, and J. Flouquet, Unusual strong spin-fluctuation effects around the critical pressure of the itinerant Ising-type ferromagnet URhAl, *Phys. Rev. B* **91**, 125115 (2015).
- [12] V. A. Sidorov, E. D. Bauer, N. A. Frederick, J. R. Jeffries, S. Nakatsuji, N. O. Moreno, J. D. Thompson, M. B. Maple, and Z. Fisk, Magnetic phase diagram of the ferromagnetic Kondo-lattice compound $CeAgSb_2$ up to 80 kbar, *Phys. Rev. B* **67**, 224419 (2003).
- [13] H. Kotegawa, T. Toyama, S. Kitagawa, H. Tou, R. Yamauchi, E. Matsuoka, and H. Sugawara, Pressure–temperature–magnetic field phase diagram of ferromagnetic Kondo lattice $CeRuPO$, *J. Phys. Soc. Jpn.* **82**, 123711 (2013).
- [14] E. Lengyel, M. E. Macovei, A. Jesche, C. Krellner, C. Geibel, and M. Nicklas, Avoided ferromagnetic quantum critical point in $CeRuPO$, *Phys. Rev. B* **91**, 035130 (2015).
- [15] J. G. Cheng, K. Matsubayashi, W. Wu, J. P. Sun, F. K. Lin, J. L. Luo, and Y. Uwatoko, Pressure Induced Superconductivity on the Border of Magnetic Order in MnP, *Phys. Rev. Lett.* **114**, 117001 (2015).
- [16] M. Matsuda, F. Ye, S. E. Dissanayake, J. G. Cheng, S. Chi, J. Ma, H. D. Zhou, J. Q. Yan, S. Kasamatsu, O. Sugino, T. Kato, K. Matsubayashi, T. Okada, and Y. Uwatoko, Pressure dependence of the magnetic ground states in MnP, *Phys. Rev. B* **93**, 100405(R) (2016).
- [17] V. Taufour, U. S. Kaluarachchi, R. Khasanov, M. C. Nguyen, Z. Guguchia, P. K. Biswas, P. Bonfà, R. De Renzi, X. Lin, S. K. Kim, E. D. Mun, H. Kim, Y. Furukawa, C.-Z. Wang, K.-M. Ho, S. L. Bud'ko, and P. C. Canfield, Ferromagnetic Quantum Critical Point Avoided by the Appearance of Another Magnetic Phase in $LaCrGe_3$ under Pressure, *Phys. Rev. Lett.* **117**, 037207 (2016).
- [18] U. S. Kaluarachchi, S. L. Bud'ko, P. C. Canfield, and V. Taufour, Tricritical wings and modulated magnetic phases in $LaCrGe_3$ under pressure, *Nat. Commun.* **8**, 546 (2017).
- [19] D. Belitz, T. R. Kirkpatrick, and T. Vojta, First Order Transitions and Multicritical Points in Weak Itinerant Ferromagnets, *Phys. Rev. Lett.* **82**, 4707 (1999).
- [20] T. R. Kirkpatrick and D. Belitz, Exponent relations at quantum phase transitions with applications to metallic quantum ferromagnets, *Phys. Rev. B* **91**, 214407 (2015).
- [21] N. T. Huy, A. Gasparini, J. C. P. Klaasse, A. de Visser, S. Sakarya, and N. H. van Dijk, Ferromagnetic quantum critical point in URhGe doped with Ru, *Phys. Rev. B* **75**, 212405 (2007).
- [22] J. Yang, B. Chen, H. Ohta, C. Michioka, K. Yoshimura, H. Wang, and M. Fang, Spin fluctuations on the verge of a ferromagnetic quantum phase transition in $Ni_3Al_{1-x}Ga_x$, *Phys. Rev. B* **83**, 134433 (2011).
- [23] K. Huang, J. J. Hamlin, R. E. Baumbach, M. Janoschek, N. Kanchanavatee, D. A. Zocco, F. Ronning, and M. B. Maple, Ferromagnetic quantum critical point in $UCo_{1-x}Fe_xGe$, *Phys. Rev. B* **87**, 054513 (2013).
- [24] A. Steppke, R. Kuchler, S. Lausberg, E. Lengyel, L. Steinke, R. Borth, T. Lühmann, C. Krellner, M. Nicklas, C. Geibel, F. Steglich, and M. Brando, Ferromagnetic quantum critical point in the heavy-fermion metal $YbNi_4(P_{1-x}As_x)_2$, *Science* **339**, 933 (2013).
- [25] Y. Lai, S. E. Bone, S. Minasian, M. G. Ferrier, J. Lezama-Pacheco, V. Mocko, A. S. Ditter, S. A. Kozimor, G. T. Seidler, W. L. Nelson, Y. C. Chiu, K. Huang, W. Potter, D. Graf, T. E. Albrecht-Schmitt, and R. E. Baumbach, Ferromagnetic quantum critical point in $CePd_2P_2$ with Pd \rightarrow Ni substitution, *Phys. Rev. B* **97**, 224406 (2018).
- [26] B. Shen, Y. Zhang, Y. Komijani, M. Nicklas, R. Borth, A. Wang, Y. Chen, Z. Nie, R. Li, X. Lu, H. Lee, M. Smidman, F. Steglich, P. Coleman, and H. Yuan, Strange-metal behaviour in a pure ferromagnetic Kondo lattice, *Nature (London)* **579**, 51 (2020).
- [27] N. J. Ghimire, F. Ronning, D. J. Williams, B. L. Scott, Y. Luo, J. D. Thompson, and E. D. Bauer, Investigation of the physical properties of the tetragonal $CeMAl_4Si_2$ ($M = Rh, Ir, Pt$) compounds, *J. Phys.: Condens. Matter* **27**, 025601 (2015).
- [28] A. Maurya, A. Thamizhavel, A. Provino, M. Pani, P. Manfrinetti, D. Paudyal, and S. K. Dhar, Synthesis, crystal and electronic structure of the quaternary magnetic $EuTAl_4Si_2$ ($T = Rh$ and Ir) compounds, *Inorg. Chem.* **53**, 1443 (2014).
- [29] See Supplemental Material at <http://link.aps.org/supplemental/10.1103/PhysRevMaterials.7.075003> for powder x-ray diffraction, low-temperature resistivity above 20 GPa, and isotherms of magnetoresistance measured at 0.3 K.
- [30] L. J. van der Pauw, A method of measuring the resistivity and Hall coefficient on lamellae of arbitrary shape, *Philips Tech. Rev.* **20**, 220 (1958).
- [31] H. K. Mao, J. Xu, and P. M. Bell, Calibration of the ruby pressure gauge to 800 kbar under quasi-hydrostatic conditions, *J. Geophys. Res. Solid Earth* **91**, 4673 (1986).
- [32] G. Seyfarth, A. S. Rüetschi, K. Sengupta, A. Georges, D. Jaccard, S. Watanabe, and K. Miyake, Heavy fermion superconductor $CeCu_2Si_2$ under high pressure: Multiprobing the valence crossover, *Phys. Rev. B* **85**, 205105 (2012).

- [33] Z. Ren, L. V. Pourovskii, G. Girit, G. Lapertot, A. Georges, and D. Jaccard, Giant Overlap between the Magnetic and Superconducting Phases of CeAu_2Si_2 under Pressure, *Phys. Rev. X* **4**, 031055 (2014).
- [34] S. L. Bud'ko, V. Zapf, E. Morosan, and P. C. Canfield, Field-dependent Hall effect in single-crystal heavy-fermion YbAgGe below 1 K, *Phys. Rev. B* **72**, 172413 (2005).
- [35] H. Wang, T. B. Park, S. Shin, H. Jang, E. D. Bauer, and T. Park, Field-induced multiple quantum phase transitions in the antiferromagnetic Kondo-lattice compound $\text{CeRhAl}_4\text{Si}_2$, *Phys. Rev. B* **105**, 165110 (2022).
- [36] T. A. Elmslie, D. VanGennep, W. Bi, Y. Lai, S. T. Weir, Y. K. Vohra, R. E. Baumbach, and J. J. Hamlin, Pressure-induced suppression of ferromagnetism in CePd_2P_2 , *Phys. Rev. B* **102**, 125146 (2020).
- [37] Y. Luo, F. Ronning, N. Wakeham, X. Lu, T. Park, Z.-A. Xu, and J. D. Thompson, Pressure-tuned quantum criticality in the antiferromagnetic Kondo semimetal $\text{CeNi}_{2-\delta}\text{As}_2$, *Proc. Natl. Acad. Sci. USA* **112**, 13520 (2015).
- [38] A. M. Hallas, C. L. Huang, B. K. Rai, A. Weiland, G. T. McCandless, J. Y. Chan, J. Beare, G. M. Luke, and E. Morosan, Complex transport and magnetism in inhomogeneous mixed valence $\text{Ce}_3\text{Ir}_4\text{Ge}_{13}$, *Phys. Rev. Mater.* **3**, 114407 (2019).
- [39] B. K. Rai, I. W. H. Oswald, W. Ban, C. L. Huang, V. Loganathan, A. M. Hallas, M. N. Wilson, G. M. Luke, L. Harriger, Q. Huang, Y. Li, S. Dzsaber, J. Y. Chan, N. L. Wang, S. Paschen, J. W. Lynn, A. H. Nevidomskyy, P. Dai, Q. Si, and E. Morosan, Low-carrier density and fragile magnetism in a Kondo lattice system, *Phys. Rev. B* **99**, 085120 (2019).